Acta Geologica Sinica (English Edition), 2021, 95(2): 355–369

Application of Strontium Isotopic Stratigraphy to Dating Marine Sedimentary Units: A Case Study from the Permian Stratotype Section in Southern China

QU Hongjun[1, 2], CHEN Shuo[1, 2, *], HAN Xing[1, 2], WANG Li[1, 2], GUAN Liqun[1, 2] and FAN Yuhai[3]

[1] *Department of Geology, Northwest University, Xi'an 710069, China*
[2] *State Key Laboratory of Continental Dynamics, Northwest University, Xi'an 710069, China*
[3] *Remote Sensing Application Institute of ARSC, Xi'an 710054, China*

Abstract: The calibration of sedimentary rock absolute dates is one of the difficulties in sedimentological and stratigraphic research. Since strontium (Sr) resides in seawater much longer (≈10^6 a) than the seawater intermixing time (≈10^3 a), the Sr isotopic composition of global seawater is uniform at any time and results in a stable system throughout geological history, based on which a global Sr isotope composition dating database has been established for age-calibration of marine strata. The Permian stratigraphic sections in the northern part of the Upper Yangtze block, southern China, record continuous marine sediments with clear stratigraphic boundaries and is suitable for stratigraphic dating of Sr isotopes. Based on sampling and Sr isotopic compositions of Permian carbonate strata in the northern part of the Upper Yangtze, a Permian Sr isotope evolution curve was established. According to the basic principles of Sr isotope stratigraphy, the global Strontium isotope age database can be used to calibrate the Permian stratigraphic dates in the northern Upper Yangtze. The results show that the Sr isotope evolution curves for the marine carbonate rocks in the Permian stratigraphic section of the Upper Yangtze present a decreasing trend from the mid-Qixia stage (P_2) to the mid-Wujiaping stage (P_3), and then rise from the middle Wujiaping stage to the end of Changxing stage (P_3). When the Permian Sr-isotope evolution curve is compared with the global Sr isotope evolution curve in the northern Upper Yangtze, the two are consistent in their long-term evolutionary trend, indicating that Permian global geological events are important controlling factors for the composition and evolution of Sr isotopes. The $^{87}Sr/^{86}Sr$ value decreased gradually in the background of large-scale regressions at the turn of middle to late Permian period, revealing that the Emeishan basalt eruption occurred near the Maokou/Wujiaping boundary (GLB). Sr-isotope stratigraphy dating was performed on the boundaries of the Qixia Formation/Maokou Formation, Maokou Formation/Wujiaping Formation (GLB), Wujiaping Formation/Changxing Formation (WCB) and the Permian/Triassic (PTB) using the Global Strontium Isotope Age Database. The results are 270.4 Ma, 261.2 Ma, 254.5 Ma and 249.7 Ma, respectively. Based on this, the eruption age of the Emeishan basalts is defined at about 261.2 Ma., which is more coincident with that acquired from other previous dating methods on the eruption age of the Emeishan basalts, and therefore proves that the application of Sr isotopic stratigraphy to dating marine sedimentary units is an effective method.

Key words: geochronology, stratigraphy, strontium isotopes, marine sediments, global correlation, Guadalupian–Lopingian, Upper Yangtze region

Citation: Qu et al., 2021. Application of Strontium Isotopic Stratigraphy to Dating Marine Sedimentary Units: A Case Study from the Permian Stratotype Section in Southern China. Acta Geologica Sinica (English Edition), 95(2): 355–369. DOI: 10.1111/1755-6724.14503

1 Introduction

The determination of the absolute age of sedimentary rocks has always been a challenge for the study of sedimentology and stratigraphy (Huang et al., 2005a; Liu et al., 2007). At present, isotopic stratigraphy and magnetic stratigraphy are the general methods, and isotopic stratigraphy is one of the effective methods. Because strontium (Sr) remains in seawater for 1 million years, which is significantly longer than the seawater intermixing time of 1000 years, Sr isotope compositions are uniformly distributed across the globe in any age (Wickman, 1948; McArthur et al., 2001, 2012; Liu, 2013). The Sr isotope composition of seawater is a function of time and is dominated by the richer radiogenic Sr produced by ancient continental silicalite weathering and the relatively lean radiogenic Sr produced by mid-oceanic ridge hydrothermal systems (Burke et al., 1982; Palmer and Edmond, 1989; Veizer et al., 1999). Various global events such as orogenic events, glacial activities, climate changes, global sea-level changes, global weathering rates, oceanic crustal growth rates, changes in mid-oceanic ridge hydrothermal systems and global extinction events are all important controlling factors for the components and evolution of the Sr isotope in seawater (Derry et al., 1992; Kaufman et al., 1993; Vérard et al., 2015). The composition and evolution of the Sr isotopes of marine sediments (carbonates, sulfates, phosphates, etc.), which stand as proxy for the original seawater, are not only

* Corresponding author. E-mail: nwu_chenshuo@163.com

http://www.geojournals.cn/dzxbcn/ch/index.aspx; https://onlinelibrary.wiley.com/journal/17556724

important means for the study of major global geological events (Derry and France-Lanord, 1996; Goddéris and Veizer, 2000; Hu et al., 2008; Huang et al., 2008; Song et al., 2015; Wierzbowski et al., 2017) and stratigraphic correlation (Huang and Zhou, 1997; Veizer et al., 1997; McArthur et al., 2001, 2012; Huang et al., 2002a, 2008, 2011;Wang et al., 2007; Hu et al., 2008; Liu et al., 2013; Mutterlose et al., 2014), but also are one of the most effective tools for determining the age of marine sediments, and there are numerous successful age determination examples (Hess et al., 1989; McArthur et al., 1994, 2001; Dingle et al., 1997; Denison et al., 1998; Walter et al., 2000; Melezhik et al., 2001; Gleason et al., 2002; Ray et al., 2003; Huang et al., 2005b; Liu et al., 2013; Ye et al., 2015). At present, global Sr-isotope composition age databases (Howarth and McArthur, 1997; Veizer et al., 1999; McArthur et al., 2001) have been established internationally.

The Permian is an important period in the formation, development and evolution of the Pangean world. There were a series of major geological events, including high-frequency drastic eustatic change of sea levels (Haq and Schutter, 2008; Qiu et al., 2014), extensive glacier activities (Veevers and Powell, 1987; Isbell et al., 2003; Chen et al., 2013), severe volcanic activities and biological extinctions (Jin et al., 1994; Wang and Sugiyama, 2000; Korte et al., 2004, 2006, 2010; Isozaki et al., 2007a, b; Heydari et al., 2008; Isozaki, 2009; Shen and Mei, 2010; Hermann et al., 2011; Shen et al., 2011; Liu et al., 2013; Song et al., 2015; Zhang et al., 2015; Ji et al., 2019; Yan et al., 2019). Sea-level changes are controlled directly or indirectly by a series of geological events such as orogenic movements, glacial activities, submarine expansions and paleoclimates (Huang et al., 2001, 2008; Coogan and Dosso, 2015; Goddéris et al., 2017; Van der Meer et al., 2017). The Sr isotopic composition and evolution of the Permian seawater can record these geological events.

The Permian marine carbonate platform in the northern part of the Upper Yangtze region records continuous marine deposits and clear stratigraphic boundaries. Previous studies have focused on the composition and evolution of the Sr isotope of the Late Permian in the Upper Yangtze region (Huang, 1997; Huang et al., 2001, 2008, 2011; Xiao et al., 2009). The composition and evolution of Permian Sr isotopes have also been studied (Lu et al., 1992; Tian and Zheng, 1995). However, the published data on Sr isotope compositions are relatively limited, and there is less analysis about the geological significance of the Sr isotope evolutionary characteristics in the Upper Yangtze region. Using sampling and Sr isotopic compositions of the Permian stratotype section in the northern part of the Upper Yangtze region, the evolutionary characteristics of Permian Sr isotopes in the Upper Yangtze region have been obtained for the purpose of evaluating the preservation value of seawater by diagenetic alterations. Based on the Sr isotope analogy in the Upper Yangtze region and global Sr isotopes, the age of the Permian stratigraphic boundaries in the Upper Yangtze region can be calibrated by comparison with the global Sr isotope composition age databases, and so this paper aims at: (1) exploring a geochemical method for determining the absolute age of sedimentary rocks, and (2) exploring a method for dating and stratigraphic division of the strata where biofossils are poorly preserved. At the same time, using Sr isotope evolution curves via the locations corresponding to the Emeishan basaltic eruption, the Emeishan basalt eruption age was determined, which is roughly equivalent to the previous eruption age of the basalt determined by zircon U-Pb (Zhong et al., 2014) and paleomagnetic data (Zheng et al., 2010), which supports the accuracy of Sr isotope dating.

Sr isotope stratigraphy is still in its infancy, and its use as a tool for dating is basically at the trial stage in China, but the development trend in recent years and huge application potential have attracted worldwide attention. Earlier workers determined the Longmenshan Devonian/ Carboniferous boundary using the Sr isotope dating method, which showed consistency with the chronological boundary determined using conodonts, but was inconsistent with the chronological boundary determined using rugose corals and ostracodes, and so use of Sr isotopes may indicate that the conodonts provide more globally comparable dating (Huang et al., 2002b). At the current research level, Sr isotope stratigraphy can at least be used as one of the auxiliary tools for dating.

2 Geological Settings

The study area is located in the Tongjiang area, Sichuan Province, China. The tectonic location is on the margin of the Upper Yangtze block, in front of the Micangshan thrust belt, with the central Sichuan gentle tectonic belt to the south and the Dabashan Mountain arc-shaped thrust belt on the northeast (Fig. 1).

The Permian in the northeastern Sichuan basin from bottom to top consists of the Middle Permian to Upper Permian, with the Lower Permian generally missing (Li et al., 2005). The Middle Permian includes the Qixia Formation and the Maokou Formation; the Upper Permian consists of the Wujiaping Formation and the Changxing Formation. The Permian directly overlies the underlying Silurian unconformably, and is in conformable contact with the overlying Triassic (Feng et al., 1996; He et al., 2013; Luo et al., 2014).

The northern margin of the Upper Yangtze was adjacent to the Mianlue Ocean in the Permian period (Fig. 2b), and was a passive continental margin of the ocean (Feng et al., 1997; Dong et al., 2015; Dong and Santosh, 2016; Mei and Liu, 2017; Qu et al., 2018). During the initial Qixia stage, a widespread marine transgression in the Yangtze region submerged the Yangtze plate, which led to the formation of carbonate rocks on the Middle Permian stable platform (Feng et al., 1993; Yang and Feng, 2000; Zhu et al., 2004; Li et al., 2020). The transgression progressed into the Maokou stage, forming an open carbonate platform, carbonate shelf-slope system and epeiric sea–hemipelagic siliceous basin system from south to north, displaying a typical passive margin. At the end of the Maokou stage, the Upper Yangtze region entered the peak of its expansion, and the Emeishan earth-shaking movement reached a climax with large-scale eruptions of

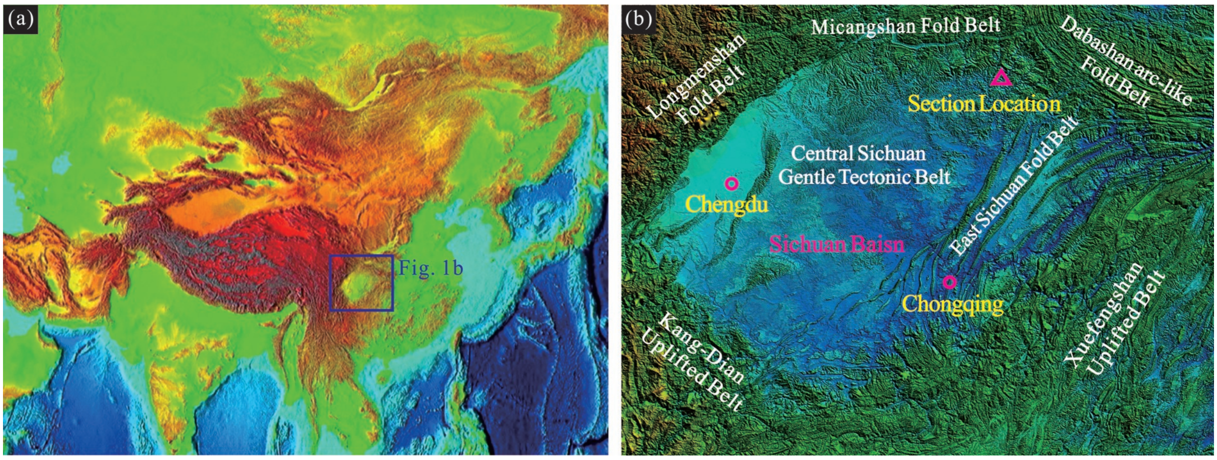

Fig. 1. Tectonic units of the study area and section location map in the Tongjiang area, Sichuan Province.
(a) Digital elevation map of China and its adjacent areas with the location of the Sichuan Basin; (b) tectonic units of the Sichuan Basin and its adjacent areas with the section location.

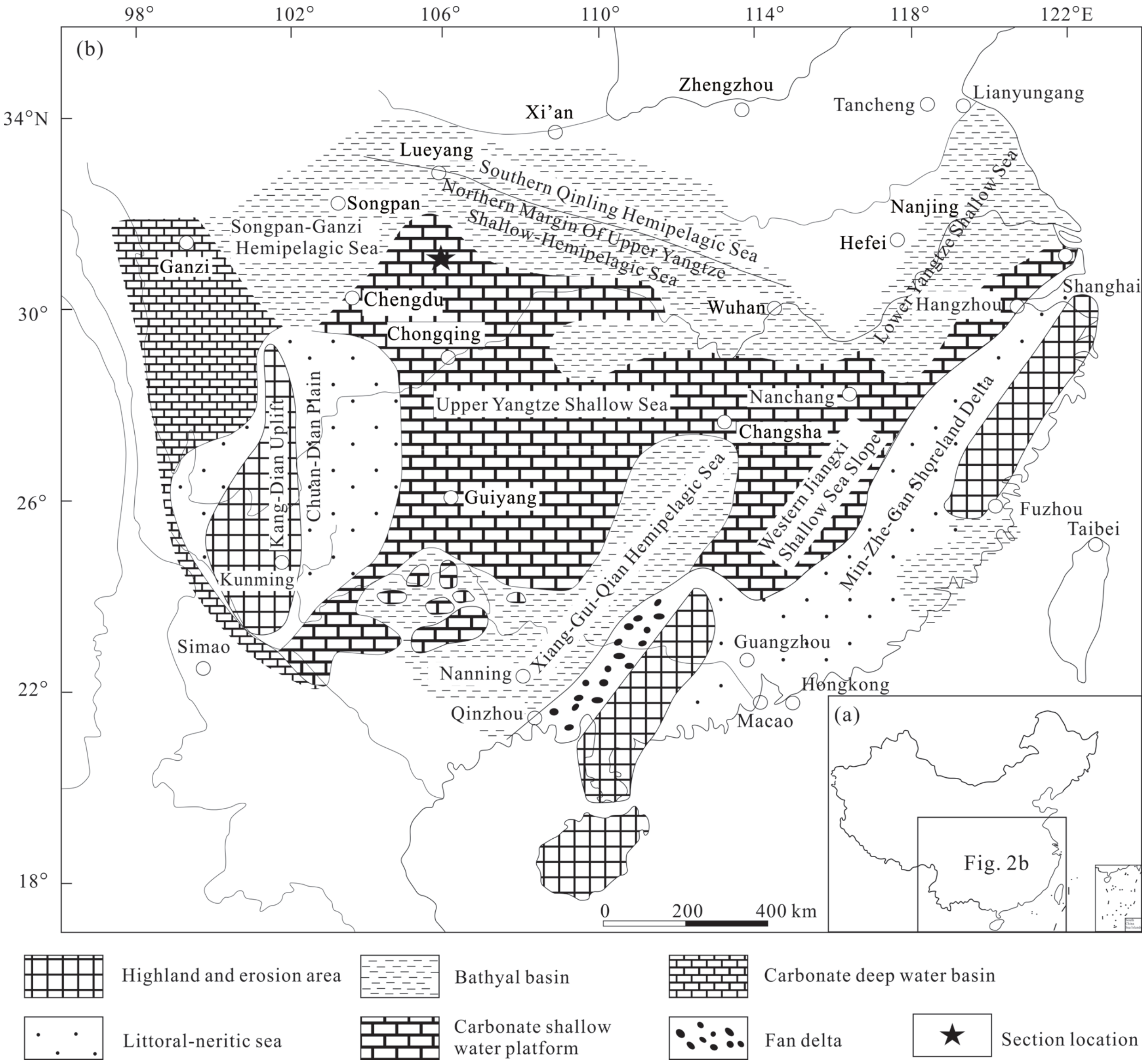

Fig. 2. Permian tectonic paleogeography map of South China and the section location (after Wang and Cai, 2007).
China basemap after the China National Bureau of Surveying and Mapping Geographical Information.

the Emeishan basalt (Zhou et al., 2002; Zhang et al., 2006; He et al., 2007; Xu et al., 2008; Zhang, 2013; Shellnutt et al., 2014; Xu et al., 2019; Zhang et al., 2019). After the Dongwu movement, which was a rapid differential crustal uplift caused by the rise of the Emeishan mantle plume, the Late Permian Mianlue ancient oceanic basin continued to expand (He et al., 2005). The initial transgression in the Wujiaping stage shows that the scale of transgression was greater in the west and smaller in the east. The central Sichuan and the southern area received coal-bearing sedimentary deposits, which are represented by the Longtan Formation (Liu et al., 2010; Shao et al., 2016), whereas carbonate sediments of the Wujiaping Formation were extensively deposited in the eastern Sichuan area. The transgression coverage in the Changxing stage expanded and also the scope of the northern deep-water basin expanded (Feng et al., 1997; Yang and Feng, 2000; Chen et al., 2002).

3 Samples and Methods

3.1 Field section sample collection and test analysis

The Permian stratigraphic section is located in the Longhudong Scenic Area about 10 km north of Pingxi Town, Tongjiang County, Sichuan Province (Fig. 3a) and, as noted above, consists in ascending order of the Qixia, Maokou, Wujiaping and Changxing formations, overlying the Silurian with disconformity and underlying the Triassic with conformity (Fig. 3b). In addition to the lack of the bottom of the Qixia Formation and a short-term depositional discontinuity between the Maokou and Wujiaping formations, the Middle to Upper Permian units represent a near-complete record of marine sedimentation, with a total thickness of 1091.1 m (Fig. 4)., A total of 102 limestone samples were collected from bottom to top in the Permian Longhudong stratotype section with an average interval of 11.7 m (Fig. 4); of these, six samples are from the Qixia Formation with a total thickness of 38.7 m, 22 samples from the Makou Formation with a total thickness of 207.3 m, 47 samples from the Wujiaping Formation with a total thickness of 372.6 m, and 27 samples from the Changxing Formation with a total thickness of 472.5 m.

Sr isotopes, Mn- and Sr-content analysis and testing were completed at the State Key Laboratory of Continental Dynamics, Northwest University, Lanzhou; 50 samples were evenly selected from 102 samples. In the Sr-isotope analysis test, 50 samples, each with a mass of ~70 mg, were crushed to 200 mesh. First, we used NH_4Ac to leach the samples, and then 2.5 mol/L of CH_3COOH in a Teflon cup to dissolve them (3h). After centrifugation, the supernatant liquid was put through an AG50W × 8 (H^+) cation exchange column with HCl as eluent; pure Sr was isolated and Sr isotope measurements were performed on a Nu Plasma multi-receiver plasma mass spectrometer. The test result of the NBS 987 standard sample is 0.710248 + 0.000024 (2s, n = 9) with a normalized value of $^{86}Sr/^{88}Sr = 0.1194$.

3.2 Strontium isotope test results

3.2.1 Sr-isotope composition and seawater representativeness assessment

Marine carbonate isotopic compositions are susceptible to later diagenetic alterations, which results in an increase in manganese (Mn) and a decrease in Sr (Veizer, 1983; Bruckschen et al., 1995). Marine carbonates with low degree of alteration tend to have a lower Mn content and a higher Sr content (Kaufman et al., 1992, 1993). Based on this, the Mn and Sr contents or the Mn/Sr ratio of marine carbonate minerals have also become one of the effective methods for judging the alteration strength of diagenetic rocks and the level to preserve original seawater information. Most of the Permian marine carbonate samples in the northern Upper Yangtze region have a lower Mn content with an average Mn content of 122.96 × 10^{-6} and a maximum content of 247 × 10^{-6}, and the Mn content of all samples is less than Korte et al. (2003)'s recommended Mn limit of 250 × 10^{-6} (Table 1). The average Sr content of all the samples was 572 × 10^{-6}, of which only one sample was less than 200 × 10^{-6}; all the other samples were larger than the minimum limit of the Sr content of 200 × 10^{-6} in the isotope stratigraphy research proposed by Derry et al. (1989) (Table 1). At the same time, the average Mn/Sr ratio of these samples is

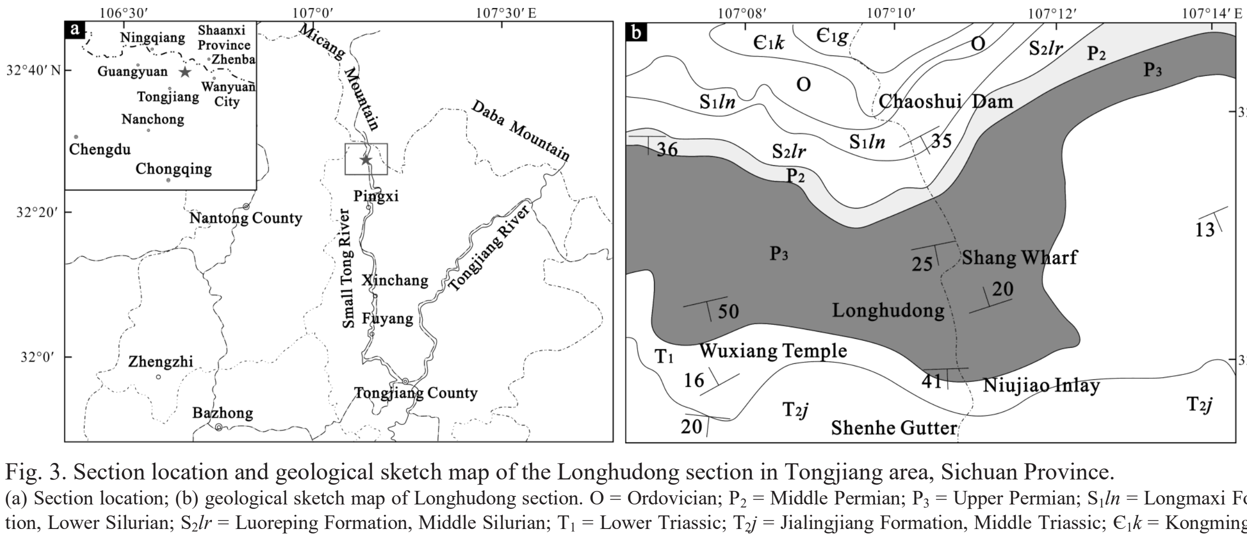

Fig. 3. Section location and geological sketch map of the Longhudong section in Tongjiang area, Sichuan Province.
(a) Section location; (b) geological sketch map of Longhudong section. O = Ordovician; P_2 = Middle Permian; P_3 = Upper Permian; S_1ln = Longmaxi Formation, Lower Silurian; S_2lr = Luoreping Formation, Middle Silurian; T_1 = Lower Triassic; T_2j = Jialingjiang Formation, Middle Triassic; $Є_1k$ = Kongmingdong Formation, Lower Cambrian; $Є_1g$ = Guojiaba Formation, Lower Cambrian.

Table 1 Statistics of strontium isotopic compositions of Permian samples in the northern Upper Yangtze region

Statum	Sample positions	Sample no.	2σ	$^{87}Sr/^{86}Sr$	Sr (ppm)	Mn (ppm)	Mn/Sr
Changxing Formation	84.8	LHD102	0.000083	0.707728	246	156	0.634
Changxing Formation	129.7	LHD101	0.00002	0.707255	365	95	0.260
Changxing Formation	162.4	LHD100	0.000013	0.707238	880	132	0.150
Changxing Formation	199.8	LHD099	0.000009	0.707212	281	45	0.160
Changxing Formation	245.8	LHD098	0.000012	0.707074	243	34	0.140
Changxing Formation	267	LHD097	0.000011	0.70711	1104	133	0.120
Changxing Formation	291.8	LHD096	0.000009	0.707201	329	125	0.380
Changxing Formation	319.1	LHD095	0.000012	0.707208	367	68	0.185
Changxing Formation	346.9	LHD094	0.00001	0.707287	289	156	0.540
Changxing Formation	397.3	LHD092	0.000008	0.707128	339	122	0.360
Changxing Formation	425.1	LHD090	0.000017	0.707287	248	67	0.270
Changxing Formation	461.2	LHD087	0.000012	0.707096	721	138	0.191
Changxing Formation	488.4	LHD085	0.000013	0.707267	655	72	0.110
Changxing Formation	506.3	LHD083	0.000009	0.707037	652	188	0.288
Changxing Formation	527.5	LHD080	0.000015	0.707101	1058	211	0.199
Changxing Formation	540.8	LHD078	0.000014	0.707185	577	247	0.428
Changxing Formation	551.1	LHD077	0.00001	0.707019	356	35	0.098
Wujiaping Formation	562.4	LHD075	0.000009	0.707096	474	189	0.399
Wujiaping Formation	576.7	LHD073	0.000011	0.707041	730	146	0.200
Wujiaping Formation	591.6	LHD071	0.000009	0.707092	262	164	0.626
Wujiaping Formation	601	LHD069	0.00001	0.707029	938	75	0.080
Wujiaping Formation	618	LHD066	0.000011	0.707102	354	99	0.280
Wujiaping Formation	629.5	LHD064	0.000011	0.707017	763	61	0.080
Wujiaping Formation	644.8	LHD062	0.000012	0.707017	418	39	0.093
Wujiaping Formation	659.5	LHD060	0.000017	0.707381	526	163	0.310
Wujiaping Formation	684.4	LHD057	0.000008	0.707134	1245	192	0.154
Wujiaping Formation	707.4	LHD053	0.000015	0.707122	342	82	0.240
Wujiaping Formation	732	LHD049	0.000011	0.707012	888	91	0.102
Wujiaping Formation	741.9	LHD047	0.000008	0.707037	544	97	0.178
Wujiaping Formation	744.8	LHD046	0.000012	0.707074	356	123	0.346
Wujiaping Formation	782.4	LHD043	0.000012	0.707245	630	222	0.352
Wujiaping Formation	806.5	LHD040	0.000011	0.707042	1100	77	0.070
Wujiaping Formation	825.2	LHD037	0.00002	0.707206	634	78	0.123
Wujiaping Formation	837.7	LHD035	0.00002	0.707339	322	145	0.450
Wujiaping Formation	843.9	LHD034	0.00001	0.707297	263	42	0.160
Wujiaping Formation	909	LHD032	0.00001	0.707026	244	88	0.361
Wujiaping Formation	920.9	LHD031	0.000012	0.70703	195	43	0.221
Wujiaping Formation	924.8	LHD030	0.000012	0.707083	267	88	0.330
Maokou Formation	946.6	LHD028	0.000014	0.7071	359	147	0.409
Maokou Formation	975.9	LHD025	0.000013	0.707121	726	89	0.123
Maokou Formation	992.1	LHD023	0.000011	0.707084	741	215	0.290
Maokou Formation	1017.7	LHD020	0.000296	0.70708	756	176	0.233
Maokou Formation	1034.8	LHD018	0.000011	0.707073	550	77	0.140
Maokou Formation	1051.9	LHD016	0.000012	0.707279	1236	194	0.157
Maokou Formation	1086.9	LHD013	0.000012	0.707446	882	97	0.110
Maokou Formation	1113.4	LHD010	0.000015	0.707568	527	92	0.175
Maokou Formation	1131	LHD008	0.000258	0.707276	340	85	0.250
Maokou Formation	1148.7	LHD006	0.00001	0.707337	418	230	0.550
Qixia Formation	1166.9	LHD003	0.000012	0.70812	1205	229	0.190
Qixia Formation	1177.5	LHD001	0.00001	0.708235	676	169	0.250

0.25, which is much lower than the upper limit Mn/Sr value (2~3) of the sample in the Sr isotope stratigraphy study proposed by Kaufman et al. (1992, 1993). In addition, there was no correlation between the $^{87}Sr/^{86}Sr$ ratio, the Mn content, Sr content, and Mn/Sr value in the samples (Fig. 5). In conclusion, the Permian marine carbonate rocks in the northern part of the Upper Yangtze have a high Sr content, low Mn content and Mn/Sr values, and mostly preserve the original information of sea water.

The results of isotopic compositions of Permian marine carbonate in the Upper Yangtze reveal that the $^{87}Sr/^{86}Sr$ data for all samples ranges from 0.707072 to 0.708235, with an average of 0.707211 and an average uncertainty of 0.000024. Compared to the ranges of the Sr-isotope composition (0.706837–0.708190) of the Permian synchronizing brachiopod fossils of Popp et al. (1986), only one of the Sr-isotope data exceeds this range (Table 1). It can be seen that the Sr-isotope data obtained by this test analysis are consistent with geological facts of the Permian in the study area, and the distribution is also more reasonable.

In addition to the above geochemical analysis, the effect of sample diagenesis on the applicability of the Sr-isotope method is also considered from the perspective of petrology and mineralogy. The lithology of the nos. 1–33 strata in the section is mainly limestone (Fig. 4), a few of which are dolomitic. Only the top nos. 34–37 strata are dolostone, which has a uniform microcrystalline structure, where the dolomite had completely replaced the calcite and there was no residual calcite (Fig. 6), which could reflect penecontemporaneous dolomitization metasomatic diagenesis. Therefore, the dolostone was formed in an

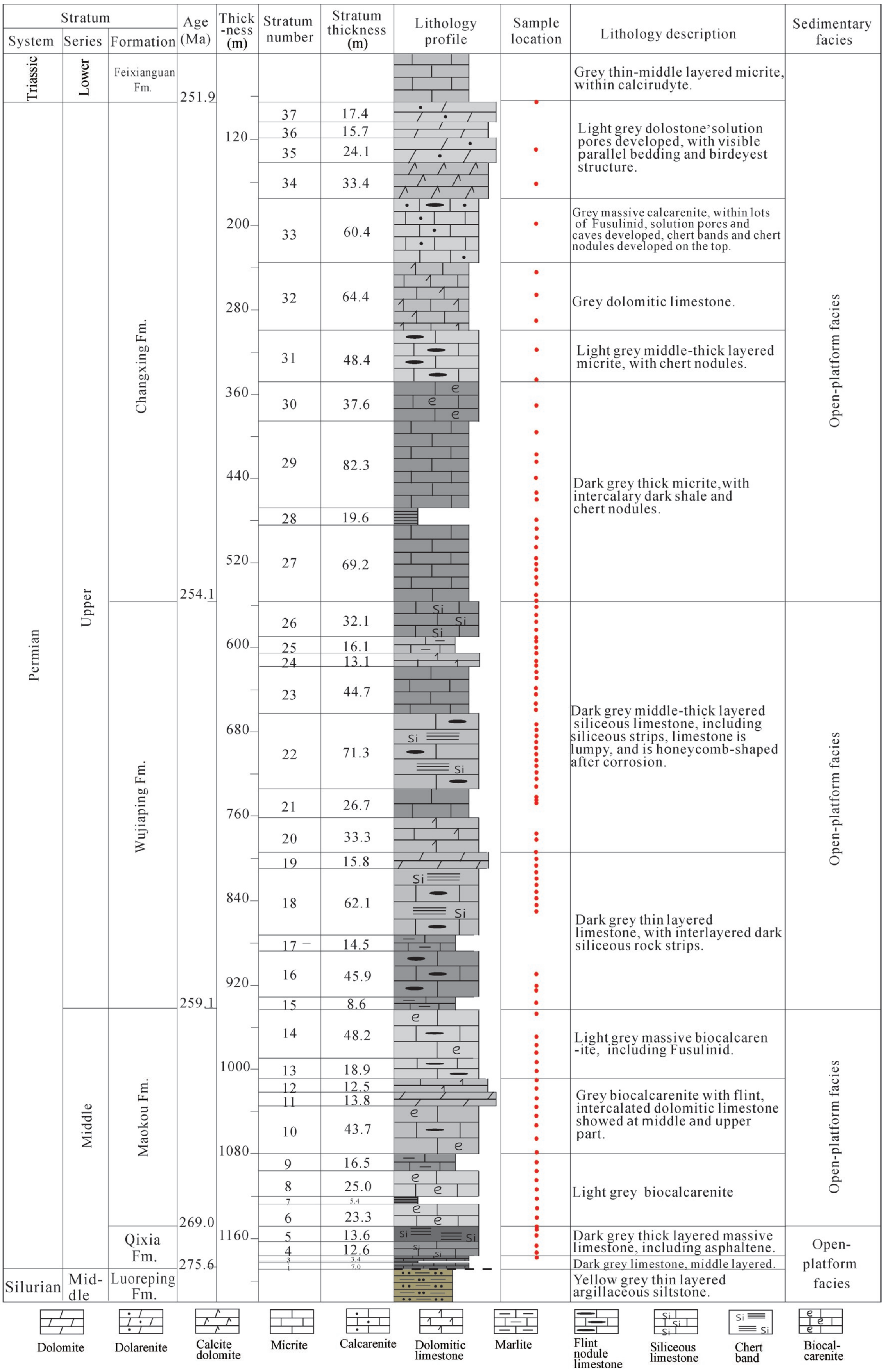

Fig. 4. Permian composite columnar section and sampling positions in the northern Upper Yangtze Region.

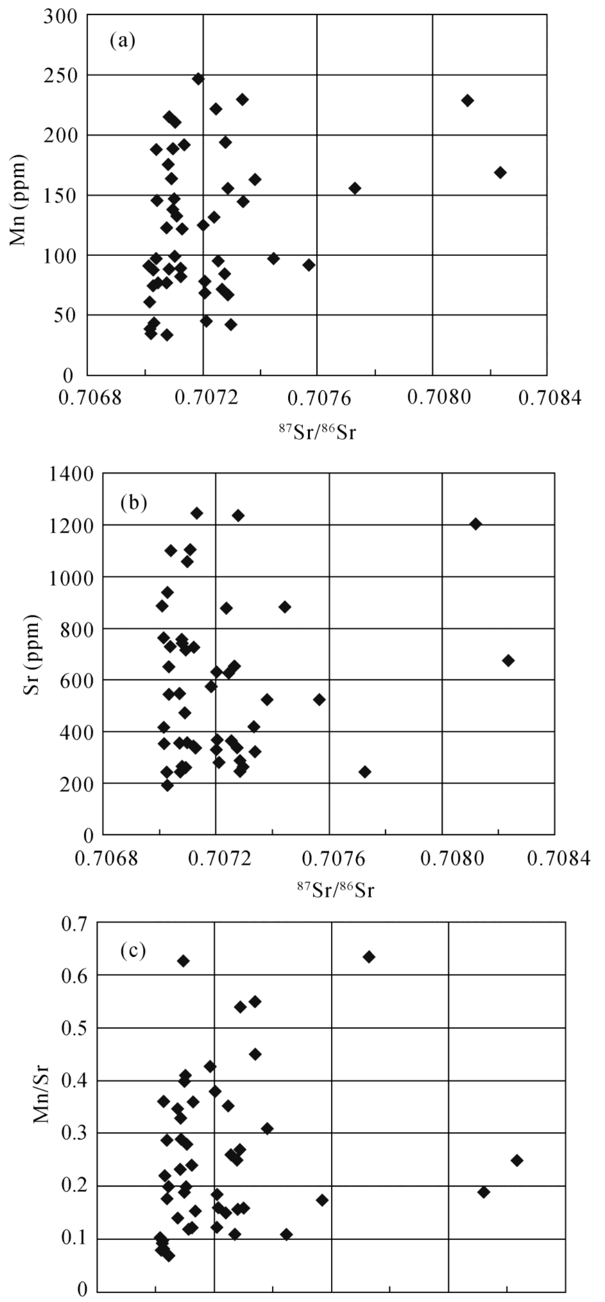

Fig. 5. Sr-isotopic ratios and correlation diagrams of Mn contents, Sr contents, and Mn/Sr ratios. (a) Sr-isotopic ratios versus Mn contents; (b) Sr-isotopic ratios versus Sr contents; (c) Sr-isotopic ratios versus Mn/Sr ratios.

open system environment, and the Sr in the formation water represents that in the composition of the original seawater, and the penecontemporaneous metasomatic dolostone can be used to study the Sr-isotope stratigraphy, so it can be used for the determination of the age of the strata (Huang et al., 2011). However, secondary metasomatic dolomite formed by late diagenesis was formed in a closed system, and so it can not be used for the determination of Sr-isotope stratigraphic age.

Previous studies on Sr-isotopic composition of the Upper Permian–Lower Triassic dolomites in the northeastern Sichuan Basin showed similar evolutionary trends with that of seawater in the same period, combined with the low Mn and high Sr characteristics of the dolomites, which demonstrated a significant genetic relationship between the dolomitization fluids and coeval seawater; the Sr in the dolomitization fluids can basically represent the isotopic composition of the coeval seawater (Huang et al., 2011).

Due to the development of the siliceous rock strips in the study section, we need to consider whether Sr-isotope analysis can be used to research silicites. In fact, many previous such studies had been carried out (Shen et al., 1981; Huang et al., 1999; Lu et al., 2004), and confirmed the applicability of the method. For example, Huang et al. (1999) compared the Sr-isotopic composition evolution curve of Carboniferous–Permian deep-water silicites in the Qinzhou trough, Guangxi province, with that of the Upper Yangtze platform carbonate, finding that the overall trends of the two were the same, although the Sr-isotopic composition of the siliceous rocks was generally high.

3.2.2 Sr-isotope evolution curve and its global comparison

Based on the sampling positions and $^{87}Sr/^{86}Sr$ cast points, the LOWESS method was used to fit the Sr-isotope data. The $^{87}Sr/^{86}Sr$ values show changes from the early stage of the Middle Permian to the turn of the Permian–Triassic (PTB) (Fig. 7). The Permian Sr-isotope evolution curve in the northern Upper Yangtze shows an overall trend of decreasing first and then increasing. It decreased from the Qixia stage to the middle Wujiaping stage, then gradually increased from the middle Wujiaping to the end Changxing stages, and especially increased abruptly at the end of the Late Permian.

The Sr-isotope curve of the Qixia stage shows a decreasing trend; the initial $^{87}Sr/^{86}Sr$ value is 0.708235, while by the late Qixia stage, the $^{87}Sr/^{86}Sr$ value becomes 0.707337, with the descending rate being 0.0001/10m. The Sr-isotope curve then moves higher at the beginning of the Maokou stage, with the $^{87}Sr/^{86}Sr$ value reaching 0.707568, and then gradually shifting to a lower value, while at the end of the stage, gradually decreasing to 0.707073. In the early to middle stage of the Wujiaping stage, the Sr-isotope curve shows two small peaks, reaching a minimum value of 0.707012 at the middle of the stage, and also forming a trough between the two small peaks, which is also the lowest point in the Permian Sr-isotope composition curves. After this, the curve remains relatively stable, maintaining at around 0.707115. The Sr-isotope evolution curve in the early Changxing stage inherited the stable evolutionary characteristics of the Wujiaping stage, shifting to a high value of 0.707287 in the middle of the stage, and then to a lower value at almost the same rate, reaching a low value of 0.707074 in the late Changxing stage, finally beginnning to shift toward a higher value. The $^{87}Sr/^{86}Sr$ rapidly increased from 0.707255 to 0.707728 at the end of the Changxing stage, at the turn of the PTB, with an average increasing rate of

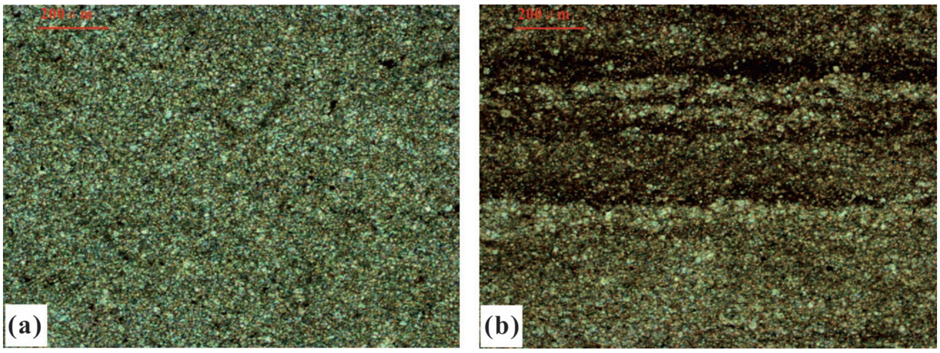

Fig. 6. Microscope photographs of dolomites at the top of the Changxing Formation (P_3) in the Longhudong section, Tongjiang area, Sichuan Province.
(a) Microcrystalline dolomite (10×); (b) lamellar microcrystalline dolomite (10×).

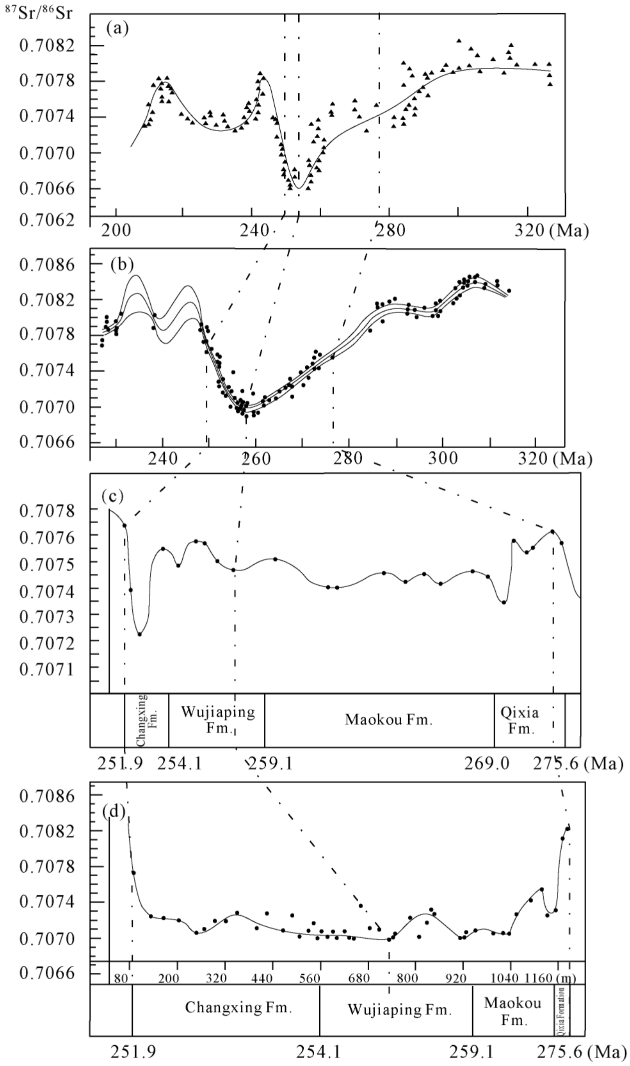

Fig. 7. Comparison of strontium isotope composition evolution curve of the Permian in the northern Upper Yangtze Region with the global Sr-isotope curve.
(a) The global Sr isotope curve (Veizer et al., 1999); (b) the global Sr-isotope evolution curve of 225–320 Ma (McArthur et al., 2001); (c) Permian paleo-ocean Sr-isotope composition evolution curves in South China (Tian and Zheng, 1995); (d) Sr-composition evolution curves of the Permian in the northern Upper Yangtze Region; geological dates based on the Permian Timescale (after Cohen et al., 2020).

0.0001/10 m (Fig. 7).

The Sr-isotopic compositions have obvious changes at the geological boundaries, showing troughs at the three formation boundaries, equivalent to the Guadalupian–Lopingian boundary (GLB), while appearing as peaks at the boundaries of the Wujiaping to Changxing formations and at the PTB (Fig. 7).

Comparing the northern Upper Yangtze Permian Sr-isotope evolution curve with that of south China and also the global Permian Sr-isotope curve (Fig. 7), it can be seen that there are some differences between them but, in general, good agreement in the long term evolutionary trend of the northern Upper Yangtze Sr-isotope evolution curve with the internationally accepted curve is displayed (Figs. 7a, b, d), and also good similarity with that of southern China (Figs. 7c, d), which indicates that global geological events are the most important controlling factors for the composition and evolution of marine carbonate Sr isotopes.

The Sr-isotope ratio decreased gradually from 0.708235 to 0.707026 from the Middle Permian to Early Permian in the study area, following the Sr-isotope evolution curve elsewhere that also gradually decreased during this period (Veizer et al., 1999; McArthur et al., 2001, 2012). The Sr-isotope data in the middle stage of the Late Permian gradually increased from 0.707026 to 0.707255 in the study area, agreeing with $^{87}Sr/^{86}Sr$ values elsewhere that also tended to increase steadily during this period (Veizer et al., 1999; McArthur et al., 2001, 2012), with $^{87}Sr/^{86}Sr$ values being linearly correlated with time (Veizer et al., 1999; Williamson et al., 2012; Liu et al., 2013; Ye et al., 2015). The Sr-isotope ratio increased sharply from 0.707255 to 0.707728 at the end of the Late Permian and at the turn of the PTB, just as the curve determined elsewhere (Veizer et al., 1999; McArthur et al., 2001, 2012; Shen and Mei, 2010).

It should be noted that the minimum Sr-isotopic composition since the Paleozoic occurred in the late Guadalupian (Maokou stage), with the $^{87}Sr/^{86}Sr$ being around 0.70687 (Veizer et al., 1999; McArthur et al., 2001; Korte et al., 2003, 2006; Kani et al., 2008, 2013; Isozaki, 2009), while the minimum $^{87}Sr/^{86}Sr$ in the Permian Upper Yangtze region occurred in the Wujiaping stage (Huang et al., 2008). The minimum value of the Sr-isotope ratio of this study appears in the middle of Wujiaping stage, with a value of 0.707012. During the Emeishan basaltic eruption period, large igneous province large-scale eruptions (especially underwater) greatly increased the lean-radioactive origin Sr contribution, causing a decrease in seawater $^{87}Sr/^{86}Sr$ value, which eventually reduced to 0.707026 in the early Wujiaping stage. Extensively distributed terrigenous outpouring basalts, which have undergone long-term weathering and surface runoff leaching, carried large amounts of basalt into the oceans (Lu et al., 1992), causing the Sr-isotope composition of seawater to eventually reach a minimum in the middle of the Wujiaping stage.

4 Discussion on Age Calibration

Sr-isotope dating of marine strata requires extensive accumulations of Sr-isotope data representing seawater information on the basis of high-precision Sr-isotope analysis testing and the establishment of a representative global Sr-isotope-age database for age dating (Huang et al., 2002b, 2005a; Liu et al., 2007; Wang et al., 2014). McArthur et al. (2001) collected much Sr-isotope data, with lower diagenetic alteration in the samples and high accuracy in analyses, and used the best LOWESS method to establish a global 0–509 Ma Sr-isotope age database for marine strata dating. The age calibration of the Permian stratigraphic boundaries in our study was achieved by casting the Sr-isotope composition value of each boundary onto the Permian Sr-isotope evolution curve established by McArthur et al. (2001).

4.1 Stratigraphic boundary age calibration

4.1.1 Qixia–Maokou Formation boundary age calibration

The casting data were selected from testing data of the three samples LHD006, LHD008 and LHD010 near the boundary of the Qixia Formation and the Maokou Formation, with the $^{87}Sr/^{86}Sr$ values of the samples being 0.707337, 0.707276 and 0.707568 respectively. These samples had a low Mn content and a high Sr content with a low Mn/Sr ratio (Table 1), which can represent well the seawater Sr-isotope composition. The mean $^{87}Sr/^{86}Sr$ value for the three samples is 0.707394, which compared with the Sr isotope-age database curve of McArthur et al. (2001), supports the boundary line date of the Qixia to Maokou Formation boundary of 270.4 Ma (Fig. 8).

4.1.2 Maokou–Wujiaping Formation boundary (GLB) age calibration

The casting data were selected from four samples LHD028, LHD030, LHD031 and LHD032 near the boundary of Maokou and Wujiaping formations, with the $^{87}Sr/^{86}Sr$ values being 0.707100, 0.707083, 0.707030 and 0.707026, respectively. All four samples had low Mn content, high Sr content and a low Mn/Sr ratio (Table 1), mirroring the composition of the seawater age database of McArthur et al. (2001), supports a boundary line date for the Maokou–Wujiaping Formation (GLB) of 261.2 Ma (Fig. 8).

Zhong et al. (2014), using a CA-TIMS U-Pb age

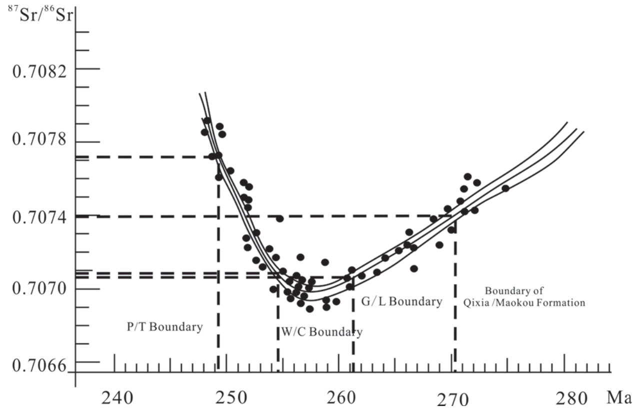

Fig. 8. Projection ages of the Sr-isotopic composition of several stratigraphic boundaries on the Permian Sr-isotopic evolution curve (database after McArthur et al., 2001).

analysis to study the basalts and volcaniclastic rocks in Binchuan, Yunnan Province, suggested that the Guadalupian and Leping Lopingian epoch boundary (GLB) age is 259.1 ± 0.5 Ma, which is only 1.9 Myr discrepancy from that for the Maokou–Wujiaping boundary line (GLB) calibrated in this study.

4.1.3 Wujiaping–Changxing Formation boundary (WCB) age calibration

Casting data were selected from the testing data of five samples LHD073, LHD075, LHD077, LHD078 and LHD080, with $^{87}Sr/^{86}Sr$ values near the boundary being 0.707041, 0.707096, 0.707019, 0.707185 and 0.707101, respectively. All samples had low Mn content, high Sr content and a low Mn/Sr value (Table 1), comparable with the seawater Sr-isotope composition. The average $^{87}Sr/^{86}Sr$ of the five samples was 0.707088, which when was put on the curve of the Sr-isotope-age database of McArthur et al. (2001), supports a boundary line date for the Wujiaping Formation–Changxing Formation (WCB) of 254.5 Ma (Fig. 8).

Mundil et al. (2004) determined the date for the WCB as 254.7 ± 0.2 Ma in Shangsi, Sichuan Province, and Meishan, Zhejiang Province using CA–TIMS U–Pb dating. Based on high-precision U–Pb dating, the WCB was also defined at 254.14 Ma by Shen et al. (2010, 2011), which thus gives only a 0.36 Myr discrepancy with that of the WCB date (GLB) calibrated by this study.

4.1.4 Permian–Triassic boundary (PTB) age calibration

The PTB, i.e., the boundary between the Changxing Formation and the Feixianguan Formation, shows an abrupt change in $^{87}Sr/^{86}Sr$ (Fig. 8), and the samples here are relatively sparse. If average $^{87}Sr/^{86}Sr$ of the nearby boundary samples, as mentioned above, are selected, great inaccuracy might ensue. Therefore, for calibrating a sample selection at the P/T boundary, only LHD102 at the boundary was selected, with an $^{87}Sr/^{86}Sr$ value of 0.707728 (Table 1). This sample has a Mn content of 156 $\times 10^{-6}$, a Sr content of 246 $\times 10^{-6}$, and a Mn/Sr ratio of 0.63. It can be seen that the sample did not undergo strong alteration and can represent the original Sr-isotope composition of seawater. The $^{87}Sr/^{86}Sr$ ratio of this sample was casted on the curve of the Sr-isotope composition–age database (McArthur et al., 2001), with a date of 249.7 Ma (PTB) obtained (Fig. 8).

Shen et al. (2011) determined that the P/T boundary dates for the Shangsi section and Meishan section as 252.25 ± 0.12 Ma and 252.17 ± 0.06 Ma, respectively, based on stratigraphic contrast and absolute age constraints. Burgess et al. (2014) re-measured a single grain zircon in the upper and lower clay layers of the PTB at Meishan and determined that the P/T boundary line age was 251.902 ± 0.24 Ma, with only a 2.2 Myr discrepancy as calibrated by this study of the PTB.

Most of the dating results using Sr stratigraphy coincide with the ages of the international standard strata, with few discrepancies in individual results. The main reasons for those discrepancies are as follows: firstly, sample denaturation makes a sample have a different Sr-isotope information preservation degree from original seawater; secondly, the accuracy of instruments and separation and purification technology of the Sr-isotopes in the analysis processes bring discrepancies in the Sr-isotope datings; finally, the refinement of the Sr-isotope database also has an impact on the calibration of the chronology. Although the Sr-isotope-age database chosen in this study was a more improved one, still the data were derived from different testers, and therefore there will be discrepancies in the different analyses, and also few data existing in some individual time periods. Even though some time periods had more data, the data also tend to be more scattered. Therefore, there is an inevitable discrepancy in the database itself. With the development of Sr-isotope analysis and improvement in analysis accuracy, the global Sr-isotope age database will improve, and the use of Sr isotopes to date marine strata will become more mature and accurate.

4.2 Emeishan basaltic eruption age calibration

The descent of $^{87}Sr/^{86}Sr$ values of northern Upper Yangtze carbonate rocks reflects the Emeishan basalt eruptions at the end of the Maokou stage and the early stage of the Wujiaping stage. The $^{87}Sr/^{86}Sr$ values of the carbonate sediments in the early Maokou stage were relatively high, being 0.707407, and then the values gradually decreased from the late Maokou stage to the early Wujiaping stage reaching a relatively low value of 0.707026. After that, the $^{87}Sr/^{86}Sr$ value began to increase gradually, which reflected the influence of the Emeishan basalt eruptions on the Sr isotopes in the ancient seawater (Fig. 9). Therefore, the end of the Maokou stage and the beginning of the Wujiaping (GLB) can be correlated with the Emeishan basaltic eruptions dated at about 261.2 Ma.

The Sr-isotope composition of seawater reflects the degree of eruptions in a large igneous province (LIP) or the weathering degree of the ancient land. The rise of a mantle plume at Mount Emei at the end of the Middle Permian resulted in the rapid uplift of the surface of the Yangtze region and a rapid and large-scale regression (Isozaki et al., 2008; Xu et al., 2008; Chen et al., 2009). The basaltic melts in the deep interior of the earth broke through the crustal weakness to the surface, leading to the Emeishan basalt eruptions (Hou et al., 2006; He et al., 2007; Xu et al., 2008; Sun et al., 2010). Under the background of the large-scale regression, a large amount of crust-derived Sr generated by the weathering and denudation of the greatly exposing land surface entered the seawater. Influenced by the Emeishan basalt eruptions, a large amount of mantle-derived Sr from seawater with lower $^{87}Sr/^{86}Sr$ values from the deep crust was produced, or the basaltic rocks subjected to sea bed weathering after their accumulation made some of the lower value $^{87}Sr/^{86}Sr$ Sr transfer to the seawater. The mantle-source Sr counteracts the high $^{87}Sr/^{86}$ value of crust-source Sr brought by continental crust weathering, resulting in a slight decrease in $^{87}Sr/^{86}Sr$ values in seawater.

The Emeishan basalts had a duration of less than 1 Ma (Zhong et al., 2014). After the volcanic eruptions, widely distributed terrigenous outpourings of basalts underwent long-term weathering and surface runoff and leaching carried a large amount of basalts into the ocean, which greatly increased the ratio of mantle-derived Sr in seawater (Lu et al., 1992). Therefore, the Sr-isotope evolution curves show that the $^{87}Sr/^{86}Sr$ values continued to descend with the relatively descending sea level of the Upper Yangtze region from the end of the Maokou stage to the beginning of the Wujiaping stage. After that, a new round of transgression began in the Wujaping stage (Qin et al., 1998; Wang et al., 1999) and $^{87}Sr/^{86}Sr$ values gradually increased.

Zhou et al. (2002) obtained a relatively reliable age of 259 ± 3 Ma from SHRIMP U–Pb dating of Emei basalts. U–Pb zircon dates of 261 ± 4 Ma and 262 ± 3 Ma were obtained for the black granites and dikes intruding into the Devonian strata, respectively (Guo et al., 2004). Shellnutt et al. (2012) used U–Pb dating of zircons with CA-TIMS from the femag and felsic intrusive rocks in the Emeishan LIP, and obtained isotopic ages of 257.6 ± 0.5 Ma to 259.6 ± 0.5 Ma. The SHRIMP U–Pb isotopic age of the Wangpo shale volcanic zircon from the GLB of the Guangyuan overthrust section is 260 ± 4 Ma (He et al., 2007). The earliest eruption and maximum range/amplitude eruption time of the Emeishan basalts were determined from the conodont biozone data (Sun et al., 2010), as probably about 263.5 Ma and 260.9 Ma, respectively relative to the Permian Timescale (IUGS February 2017 edition). The Emeishan basalts erupted at 260 ± 1 Ma with a time interval of about 2 Myr (Shellnutt et al., 2014), which is roughly equivalent to the paleomagnetic data (Zheng et al., 2010). U–Pb age analysis of basalts and volcaniclastic rocks CA-TIMS in the Binchuan section, Yunnan, showed that the closure age of the Emeishan basalts was 259.1 Ma (Zhong et al., 2014), which is more consistent with the calibration results for the basalt eruption dates of this study with a discrepancy of 2 Myr.

5 Conclusions

(1) The Sr-isotope evolution curves of marine carbonate rocks in the Permian stratigraphic section of the northern Upper Yangtze generally show a decrease from the Qixia stage (P_2) to the middle Wujiaping stage and ascent from

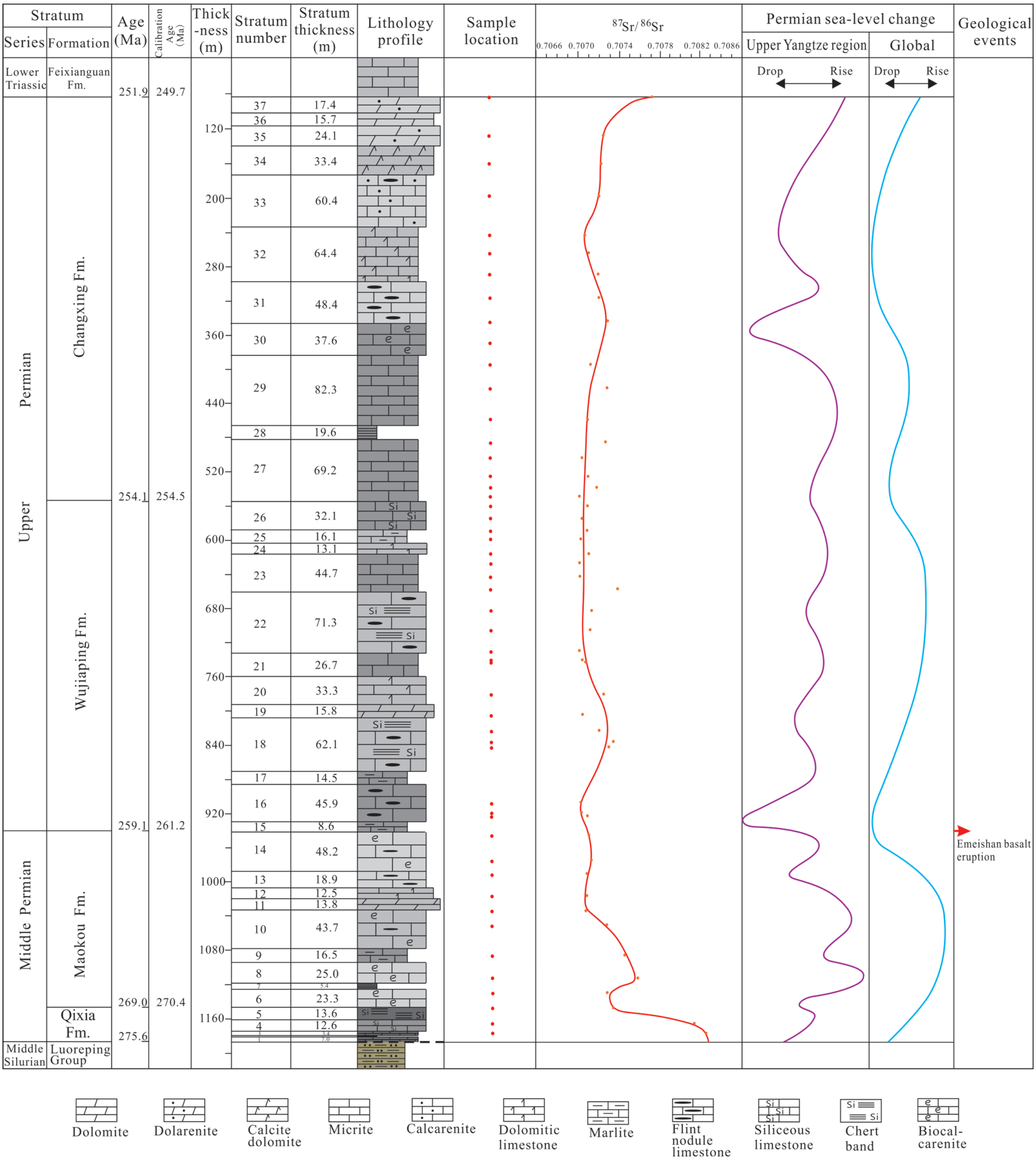

Fig. 9. Strontium stratigraphy curves of the Permian in the northern Upper Yangtze region.

The corresponding sea-level change curve in the northern Upper Yangtze region from Chen, 1995; Qin et al., 1998; Wang et al., 1999; Chen et al., 2009. The corresponding global sea-level change curve is from Haq and Schutter, 2008., and the geological age is based on the Permian Geochronometric scale (after Cohen et al., 2020).

the middle Wujiaping stage to the end of the Changxing stage (P_3). The Sr-isotope evolution curves offer good consistency with the international published global Sr-isotope evolution curves over long-term evolutionary trends, indicating that Permian global geological events are the most important controlling factors for the composition and evolution of Sr isotopes.

(2) Casting the Sr-isotope data of the Permian in the northern part of the Upper Yangtze in the global Sr-isotope composition age database, the boundary ages of the Qixia–Maokou Formation, the Maokou–Wujiaping Formation (GLB), Wujiaping–Changxing Formation

(WCB) and the Permian–Triassic Boundary (PTB) were obtained using Sr isotope stratigraphic dating method as being 270.4 Ma, 261.2 Ma, 254.5 Ma and 249.7 Ma.

(3) The Sr-isotopic evolution curves of the Permian in the northern Upper Yangtze show that the isotopic ratios of Sr gradually decrease from the end of the Maokou stage to the beginning of the Wujiaping stage (GLB), during which the Emeishan basalt eruption occurred, with an eruption age defined as about 261.2 Ma.

Acknowledgements

This work is financially supported by the National Key Research and Development Program (Grant No. 2016YFC0601003), the scientific team foundation of Department of Geology, China Northwest University, and the National Natural Science Foundation of China (Grant No. 41172101). We thank the anonymous reviewers and the editors for their constructive comments and suggestions. Dr. Susan Turner (Brisbane) assisted with English language.

Manuscript received Apr. 16, 2019
accepted Nov. 12, 2019
associate EIC: JIAN Zhimin
edited by Susan TURNER and FANG Xiang

References

Bruckschen, P., Bruhn, F., Meijer, J., and Veizer, J., 1995. Diagenetic alteration of calcitic fossil shells: proton microprobe (PIXE) as a trace element tool. Nuclear Instruments and Methods in Physics Research, 104: 427–431.

Burgess, S.D., Bowring, S.A., and Shen, S.Z., 2014. High-precision timeline for Earth's most severe extinction. Proceedings of the National Academy of Sciences of the United States of America, 111(9): 3316–3321.

Burke, W.H., Dennison, R.E., Hetherington, E.A., Koepnick, R.B., Nelson, H.F., and Otto, J.B., 1982. Variation of seawater $^{87}Sr/^{86}Sr$ throughout Phanerozoic time. Geology, 10: 516–519.

Chen, B., Joachimski, M.M., Shen, S.Z., Lambert, L.L., Lai, X.L., Wang, X.D., Chen, J., and Yuan, D.X., 2013. Permian ice volume and palaeoclimate history: oxygen isotope proxies revisited. Gondwana Research, 24(1): 77–89.

Chen, H.D., Tian, J.C., Liu, W.J., Xu, X.S., Zheng, R.C., Mu, C.L., Li, Y.S., and Qin, J.X., 2002. Division and correlation of the sequences of marine Sinian system to middle Triassic series in the south of China. Journal of Chengdu University of Technology, 29(4): 355–379 (in Chinese with English abstract).

Chen, Z.Q., 1995. The late Permian global flooding events. Sedimentary Facies and Palaeogeography, 15(3): 34–39 (in Chinese with English abstract).

Chen, Z.Q., George, A.D., and Yang, W.R., 2009. Effects of Middle–Late Permian sea-level changes and mass extinction on the formation of the Tieqiao skeletal mound in the Laibin area, South China. Australian Journal of Earth Sciences, 56 (6): 745–763.

Cohen, K.M., Harper D.A.T., Cohen, K.M., Gibbard, P.L., and Fan J.X., 2020. International Chronostratigraphic Chart 2020/03. International Commission on Stratigraphy.

Coogan, L.A., and Dosso, S.E., 2015. Alteration of ocean crust provides a strong temperature dependent feedback on the geological carbon cycle and is a primary driver of the Sr-isotopic composition of seawater. Earth and Planetary Science Letters, 415: 38–46.

Denison, R.E., Kirkland, D.W., and Evans, R., 1998. Using strontium isotopes to determine the age and origin of gypsum and anhydrite beds. The Journal of Geology, 106(1): 1–18.

Derry, L.A., and France-Lanord, C., 1996. Neogene Himalayan weathering history and river $^{87}Sr/^{86}Sr$: impact on the marine Sr record. Earth and Planetary Science Letters, 142(1–2): 59–74.

Derry, L.A., Kaufaman, A.J., and Jacobsen, S.B., 1992. Sedimentary cycling and environmental change in the Late Proeterozoic: evidence from stable and radiogenic isotopes. Geochinmica Et Cosmochimica Acta, 56(3): 1317–1329.

Derry, L.A., Keto, L.L., Jacobsen, S., Knoll, A.H., and Swett, K., 1989. Sr isotopic variations of Upper Proterozoic carbonates form East Greenland and Scalbard. Geochinmica Cosmochimica Acta, 53(9): 2331–2339.

Dingle, R.V., McArthur, J.M., and Vroon, P., 1997. Oligocene and Pliocene interglacial events in the Antarctic Peninsula dated using strontium isotope stratigraphy. Journal of the Geological Society London, 154(2): 257–264.

Dong, Y.P., and Santosh, M., 2016. Tectonic architecture and multiple orogeny of the Qinling Orogenic Belt, Central China. Gondwana Research, 29(1): 1–40.

Dong, Y.P., Zhang, X.N., Liu, X.M., Li, W., Chen, Q., Zhang, G.W., Zhang, H.F., Yang, Z., Sun, S.S., and Zhang, F.F., 2015. Propagation tectonics and multiple accretionary processes of the Qinling Orogen. Journal of Asian Earth Sciences, 104: 84–98.

Feng, Z.Z., He, Y.B., and Wu, S.H., 1993. Lithofacies paleogeography of Permian middle and lower Yangtze Region. Acta Sedimentologica Sinica, 11(3): 13–24 (in Chinese with English abstract).

Feng, Z.Z., Li, S.W., Yang, Y.Q., and Jin, Z.K., 1997. Potential of oil and gas of the Permian of South China from the viewpoint of lithofacies paleogeography. Acta Petrolei Sinica, 18(1): 11–19 (in Chinese with English abstract).

Feng, Z.Z., Yang, Y.Q., Jin, Z.K., He, Y.B., Wu, S.H., Xin, W.J., Bao, Z.D., and Tan, J., 1996. Lithofacies Paleogeography of the Permian of South China. Acta Sedimentologica Sinica, 14 (2): 1–11 (in Chinese with English abstract).

Gleason, J.D., Moore, T.C., Rea, D.K., Johnson, T.M., Owen, R.M., Blum, J.D., Hovan, S.A., and Jones, C.E., 2002. Ichthyolith strontium isotope stratigraphy of a Neogene red clay sequence: Calibrating eolian dust accumulation rates in the central North Pacific. Earth and Planetary Science Letters, 202(3–4): 625–636.

Goddéris, Y., and Veizer, J., 2000. Tectonic control of chemical and isotopic composition of ancient oceans; the impact of continental growth. American Journal of Science, 300(5): 434 –461.

Goddéris, Y., Hir, G.L., Macouin, M., Donnadieu, Y., Hubert-Théou, L., Dera, G., Aretz, M., Fluteau, F., Li, Z.X., and Halverson, G.P., 2017. Paleogeographic forcing of the strontium isotopic cycle in the Neoproterozoic. Gondwana Research, 42: 151–162.

Guo, F., Fan, W.M., Wang, Y.J., and Li, C.W., 2004. When did the Emeishan mantle plume activity start? Geochronological and geochemical evidence from ultramafic mafic dikes in southwestern China. International Geology Review, 46(3): 226–234.

Haq, B.U., and Schutter, S.R., 2008. A chronology of Paleozoic sea-level changes. Science, 322(5898): 64–68.

He, B., Xu, Y.G., Wang, Y.M., and Xiao, L., 2005. Nature of Dongwu Movement and its Temporal and Spatial evolution. Earth Science—Journal of China University of Geosciences, 30(1): 89–96 (in Chinese with English abstract).

He, B., Xu, Y.U., Huang, X.I., Shi, Y.R., Yang, Q.J., and Yu, S.Y., 2007. Age and duration of the Emeishan flood volcanism, SW China: Geochemistry and SHRIMP zircon U-Pb dating of silicic ignimbrites, post-volcanic Xuanwei Formation and clay tuff at the Chaotian section. Earth and Planetary Science Letters, 255(3): 306–323.

He, Y.B., Luo, J.X., and Wen, Z., 2013. Lithofacies palaeogeography of the Upper Permian Changxing Stage in the Middle and Upper Yangtze Region, China. Journal of Palaeogeography, 2(2): 139–162.

Hermann, E., Hochuli, P.A., Bucher, H., Brühwiler, T., Hautmann, M., Ware, D., and Roohi, G., 2011. Terrestrial ecosystems on North Gondwana following the end-Permian mass extinction. Gondwana Research, 20(2–3): 630–637.

Hess, J., Stott, L.D., Bender, M.L., Kennett, J.P., and Schilling, J.G., 1989. The Oligocene marine microfossil record: assessments using strontium isotopes. Paleoceanography, 4 (6): 655–679.

Heydari, E., Arzan, I.N., and Hassanzadeh, J., 2008. Mantle plume: The invisible serial killer — Application to the Permian–Triassic boundary mass extinction. Palaeogeography Palaeoclimatology Palaeoecology, 264(1–2): 147–162.

Hou, Z.Q., Chen, W., and Lu, J.R., 2006. Eruption of the continental flood basalts at ~ 259 Ma in the Emeishan large igneous province, SW China: evidence from laser microprobe $^{40}Ar/^{39}Ar$ dating. Acta Geologica Sinica (English Edition), 80 (4): 514–521.

Howarth, R.J., and McArthur, J.M., 1997. Statistics for strontium isotope stratigraphy: A robust LOWESS fit to marine Sr-isotope curve for 0 to 206 Ma, with look-up table for derivation of numeric age. The Journal of Geology, 105(4): 441–456.

Hu, Z.W., Huang, S.J., Qing, H.R., Wang, Q.D., Wang, C.M., and Gao, X.Y., 2008. Evolution and global correlation for strontium isotopic composition of marine Triassic from Huaying Mountains, eastern Sichuan, China. Science in China Series D: Earth Sciences, 51(4): 540–549.

Huang, S.J., 1997. A study on carbon and strontium isotopes of Late Paleozoic marine carbonates in the Upper Yangtze platform, Southwest China. Acta Geologica Sinica, 71(3): 282 –292 (in Chinese with English abstract).

Huang, S.J., and Zhou, S.H., 1997. Carbon and strontium isotopes of Late Palaeozoic marine carbonates in the upper Yangtze platform, Southwest China. Acta Geologica Sinica (English Edition), 71(3): 282–290.

Huang, S.J., Huang, Y., Lan, Y.F., and Huang K.K., 2011. A comparative study on strontium isotope composition of dolomites and their coeval seawater in the Late Permian-Early Triassic, NE Sichuan basin. Acta Petrologica Sinica, 27(12): 3831–3842 (in Chinese with English abstract).

Huang, S.J., Ma, J.M., and Leng, D.X., 1999. The strontium isotopic composition and its geological significance of deep-sea siliceous rocks from Carboniferous to Permian, Qinzhou, Guangxi. Acta Sedimentologica Sinica, 17(4): 542–546 (in Chinese with English abstract).

Huang, S.J., Qing, H.R., Huang, P.P., Hu, Z.W., Wang, Q.D., Zhou, M.L., and Liu, H.N., 2008. Evolution of strontium isotopic composition of sea-water from Late Permian to Early Triassic based on study of marine carbonates, Zhongliang Mountain, Chongqing, China. Science in China Series D: Earth Sciences, 51(4): 528–539.

Huang, S.J., Shi, H., Mao, X.D., Zhang, M., Shen, L.C., and Wu, W.H., 2002a. Evolution of Sr isotopes of the Cambrian sections in Xiushan, Chongqing, and related global correlation. Geological Review, 48(5): 509–516 (in Chinese with English abstract).

Huang, S.J., Shi, H., Shen, L.C., Zhang, M., and Wu, W.H., 2005b. Global correlation for strontium isotope curve in the Late Cretaceous of Tibet and dating marine sediments. Science in China Series D: Earth Sciences, 48(2): 199–209.

Huang, S.J., Shi, H., Zhang, M., Shen, L.C., Liu, J., and Wu, W.H., 2001. Strontium isotope evolution and global sea-level changes of Carboniferous and Permian marine carbonate, Upper Yangtze platform. Acta Sedimentologica Sinica, 19(4): 482–487 (in Chinese with English abstract).

Huang, S.J., Shi, H., Zhang, M., Wu, W.H., and Shen, L.C., 2002b. Global correlation of Strontium isotope evolution curves and dating of marine stratigraphy of Devonian in the Longmen Mountain. Progress in Natural Science, 12(9): 945–951 (in Chinese with English abstract).

Huang, S.J., Shi, H., Zhang, M., Wu, W.H., Shen, L.C., and Huang, C.G., 2005a. Strontium isotope age calibrati on of rudist bivalves from Late Cretaceous section in southern Tibet. Earth Science—Journal of China University of Geosciences, 30(1): 437–442 (in Chinese with English abstract).

Isbell, J.L., Miller, M.F., Wolfe, K.L., and Lenaker, P.A., 2003. Timing of Late Paleozoic glaciation in Gondwana: Was glaciation responsible for the development of northern hemisphere cyclothems? Geological Society of America Special Papers, 370: 5–24

Isozaki, Y., 2009. Illawarra reversal: The fingerprint of a superplume that triggered Pangean breakup and the end-Guadalupian (Permian) mass extinction. Gondwana Research, 15(3): 421–432.

Isozaki, Y., Kawahata, H., and Minoshima, K., 2007a. The Capitanian (Permian) Kamura cooling event: The beginning of the Paleozoic-Mesozoic transition. Palaeoworld, 16(1–3): 16–30.

Isozaki, Y., Shimizu, N., Yao, J., Ji, Z., and Matsuda, T., 2007b. End-Permian extinction and volcanism-induced environmental stress: The Permian-Triassic boundary interval of lower-slope facies at Chaotian, South China. Palaeogeography Palaeoclimatology Palaeoecology, 252(1–2): 218–238

Isozaki, Y., Yao, J.X., Ji, Z.S., Saitoh, M., Kobayashi, N., and Sakai, H., 2008. Rapid sea-level change in the late guadalupian (permian) on the tethyan side of south china: litho- and biostratigraphy of the chaotian section in Sichuan. Proceedings of the Japan Academy, 84(8): 344–353.

Ji, L., Liu, F.L., Wang, F., and Tian, Z.H., 2019. Depositional age, provenance characteristics and tectonic setting of the Ailaoshan Group in the Southwestern South China Block. Acta Geologica Sinica (English Edition), 93(6): 1687–1710.

Jin, Y.G., Zhang, J., and Shang, Q.H., 1994. Two phases of the end-Permian mass extinction. Pangea: Global environments and resources. Canadian Society of Petroleum Geologists, 54 (11): 1707–1711.

Kani, T., Fukui, M., Isozaki, Y., and Nohda, S., 2008. The Paleozoic minimum of $^{87}Sr/^{86}Sr$ initial ratio in the upper Guadalupian (Permian) mid-oceanic carbonates: a critical turning point in the Late Paleozoic. Journal of Asian Earth Sciences, 32(1): 22–33.

Kani, T., Hisanabe, C., and Isozaki, Y., 2013. The Capitanian (Permian) minimum of $^{87}Sr/^{86}Sr$ ratio in the mid-Panthalassan paleo-atoll carbonates and its demise by the deglaciation and continental doming. Gondwana Research, 24(1): 212–221.

Kaufman, A.J., Jacobsen, S.B., and Knoll, A.H., 1993. The Vendian record of Sr- and C-isotope variations in seawater: implications for tectonics and paleoclimate. Earth and Planetary Science Letters, 120(3–4): 409–430.

Kaufman, A.J., Knoll, A.H., and Awramik, S.M., 1992. Biostratigraphic and chemostratigraphic correlation of Neoproterozoic sedimentary successions: Upper Tindir Group, northwestern Canada, as a test case. Geology, 20(2): 181–185.

Korte, C., Jasper, T., Kozur, H.W., and Veizer, J., 2006. $^{87}Sr/^{86}Sr$ record of Permian seawater. Palaeogeography Palaeoclimatology Palaeoecology, 240(1): 89–107.

Korte, C., Kozur, H.W., Bruckschen, P., and Veizer, J., 2003. Strontium isotope evolution of Late Permian and Triassic seawater. Geochimica Et Cosmochimica Acta, 67(1): 47–62.

Korte, C., Kozur, H.W., Joachimski, M..M, Strauss, H., Veizer, J., and Schwark, L., 2004. Carbon, sulfur, oxygen and strontium isotope records, organic geochemistry and biostratigraphy across the Permian/Triassic boundary in Abadeh, Iran. International Journal of Earth Sciences, 93(4): 565–581.

Korte, C., Pande, P., Kalia, P., Kozur, H.W., Joachimski, M.M., and Oberhänsli, H., 2010. Massive volcanism at the Permian-Triassic boundary and its impact on the isotopic composition of the ocean and atmosphere. Journal of Asian Earth Sciences, 37(4): 293–311.

Li, G.H., Li, X., Song, S.Y., Song, W.H., and Yang, X.N., 2005. Dividing Permian into three series and its significance in Sichuan Basin. Natural Gas Exploration and Development, 28 (3): 20–25 (in Chinese with English abstract).

Li, M.L., Tan, X.C., Su, C.P., Lu, F.F., Zhang, B.J., Pan, Z.Y., and Xiao, D., 2020. Characteristics and genesis of sucrosic dolomite in Middle Permian Chihsia Formation, Northwest Sichuan Basin: A case study from Shangsi section. Geological Review, 66(3): 591–610 (in Chinese with English abstract).

Liu, G., 2013. Geochemistry character of strontium isotope and its application to the analysis of sedimentary environment. Acta Geologica Sinica (English Edition), 87(z1): 255–257.

Liu, H.N., Huang, S.J., Hu, Z.W., Wu, M., and Wang, Q.D.,

2007. Advances of strontium isotope in sedimentology. Lithologic Reservoirs, 19(3): 59–65 (in Chinese with English abstract).
Liu, X.C., Wang, W., Shen, S.Z., Gorgij, M.N., Ye, F.C., Zhang, Y.C., Furuyama, S., Kano, A., and Chen, X.Z., 2013. Late Guadalupian to Lopingian (Permian) carbon and strontium isotopic chemostratigraphy in the Abadeh section, central Iran. Gondwana Research, 24(1): 222–232.
Liu, X.T., Ma, Z.X., and Yan, J.X., 2010. Sedimentary environments and controlling factors of hydrocarbon source rocks of Late Permian Wujiaping Age in Yangtze area. Journal of Palaeogeography, 12(2): 244–252 (in Chinese with English abstract).
Lu, W.C., Cui, B.Q., Yang, S.Q., and Zhang, P., 1992. Strontium isotopic evolution of the Permian marine carbonates and implications. Journal of Mineralogy and Petrology, 12(4): 80–87 (in Chinese with English abstract).
Lu, Z.C., Liu, C.Q., Liu, J.J., and Wu, F.C., 2004. Geochemical studies on the Lower Cambrian witherite-bearing cherts in the northern Daba Mountains. Acta Geologica Sinica, 78(3): 390–406 (in Chinese with English abstract).
Luo, J.X., He, Y.B., and Wang, R., 2014. Lithofacies palaeogeography of the Late Permian Wujiaping Age in the Middle and Upper Yangtze Region, China. Journal of Palaeogeography, 3(4): 384–409.
McArthur, J.M., Howarth, R.J., and Bailey, T.R., 2001. Strontium isotope stratigraphy: LOWESS version 3: Best fit to the marine Sr-isotope curve for 0–509 Ma and accompanying look-up table for deriving numerical age. The Journal of Geology, 109(2): 155–170.
McArthur, J.M., Howarth, R.J., and Shields, G.A., 2012. Chapter 7 - Strontium isotope stratigraphy. In: Gradstein, F.M., Ogg, J.G., and Smith, A.G. (eds.), The Geological Time Scale, Cambridge: Cambridge University Press, 127–144.
McArthur, J.M., Kennedy, W.J., Chen, M., Thirlwall, M.F., and Gale, A.S., 1994. Strontium isotope stratigraphy for the Late Createaceous time: Direct numerical calibration of the Sr-isotope curve based on the US Western Interior. Palaeogeography Palaeoclimatology Palaeoecology, 108(1–2): 95–119.
Mei, M.X., and Liu, S.F., 2017. The Late Triassic Sequence-Stratigraphic Framework of the Upper Yangtze Region, South China. Acta Geologica Sinica (English Edition), 91(1): 51–75.
Melezhik, V.A., Gorokhov, I.M., Fallick, A.E., and Gjelle, S., 2001. Strontium and carbon isotope geochemistry applied to dating of carbonate sedimentation: An example from high-grade rocks of the Norwegian Caledonides. Precambrian Research, 108(3): 267–292.
Mundil, R., Ludwig, K.R., Metcalfe, I., and Renne, P.R., 2004. Age and timing of the Permian mass extinctions: U/Pb dating of closed-system zircons. Science, 305(5691): 1760–1763.
Mutterlose, J., Bodin, S., and Fähnrich, L., 2014. Strontium-isotope stratigraphy of the Early Cretaceous (Valanginiane Barremian): Implications for Boreale Tethys correlation and paleoclimate. Cretaceous Research, 50(2): 252–263.
Palmer, M.R., and Edmond, J.M., 1989. The strontium isotope budget of the modern ocean. Earth and Planetary Science Letters, 92(1): 11–26.
Popp, B.N., Anderson, T.F., and Sandberg, P.A., 1986. Textural, elemental and isotopic variations among constituents in Middle Devonian Limestones, North America. Journal of Sedimentary Research, 56(5): 715–727.
Qin, J.X., Chen, H.D., and Tian, J.C., 1998. The global sea-level changes during the Permian. Sedimentary Facies and Palaeogeography, 18(6): 40–47 (in Chinese with English abstract).
Qiu, Z., Wang, Q.C., Zou, C.N., Yan, D.T., and Wei, H.Y., 2014. Transgressive-regressive sequences on the slope of an isolated carbonate platform (Middle-Late Permian, Laibin, South China). Facies, 60(1): 327–345.
Qu, H.J., Li, P., Luo, T.W., Guan, L.Q., Fan, Y.H., and Wang, L., 2018. Carbon Isotopic Evolution Characteristics and the Geological Significance of the Permian Carbonate Stratotype Section in the Northern Upper–Yangtze Region, Southern China. Acta Geologica Sinica (English Edition), 92(6): 2367–2381.
Ray, J.S., Veizer, J., and Davis, W.J., 2003. C, O, Sr and Pb isotope systematics of carbonate sequences of the Vindhyan Supergroup, India: Age, diagenesis, correlations and implications for global events. Precambrian Research, 121(1–2): 103–140.
Shao, L.Y., Zhang, C., Yan, Z.M., Dong, D.X., Gao, C.X., Li, Y.J., Xu, X.Y., Liang, W.L., Yi, T.S., Xu, X.H., Li, G.M., Chen, Z.S., and Cheng, A.G., 2016. Sequence-palaegeography and coal accumulation of the Late Permian in South China. Journal of Palaeogeography, 18(6): 905–919 (in Chinese with English abstract).
Shellnutt, J.G., Bhat, G.M., Wang, K.L., Brookfield, M.E., Jahn, B.M., and Dostal, J., 2014. Petrogenesis of the flood basalts from the Early Permian Panjal Traps, Kashmir, India: Geochemical evidence for shallow melting of the mantle. Lithos, 204(3): 159–171.
Shellnutt, J.G., Denyszyn, S.W., and Mundil, R., 2012. Precise age detemination of mafic and felsic intrusive rocky from the Permian Emeishan large igneous province (SW China). Gondwana Research, 22(1): 118–126.
Shen, Q.H., Zhang, Z.Q., Xia, M.X., Wang, X.Y., and Lu, J.Y., 1981. Rb-Sr determination on the late Archean ferrosiliceous rock series in Sijiaying, Luanxian, Hebei. Geological Review, 27(3): 207–212 (in Chinese with English abstract).
Shen, S.Z., and Mei, S.L., 2010. Lopingian (Late Permian) high-resolution conodont biostratigraphic in Iran with comparison to South China zonation. Geological Journal, 45(2–3): 135–161.
Shen, S.Z., Crowley, J.L., Wang, Y., Bowring, S.A., Erwin, D.H., Sadler, P.M., Cao, C.Q., Rothman, D.H., Henderson, C.M., Ramezani, J., Zhang, H., Shen, Y.A., Wang, X.D., Wang, W., Mu, L., Li, W.Z., Tang, Y.G., Liu, X.L., Liu, L.J., Zeng, Y., Jiang, Y.F., Jin, Y.G., 2011. Calibrating the End-Permian mass extinction. Science, 334(6061): 1367–1372.
Shen, S.Z., Henderson, C.M., Bowring, S.A., Cao, C.Q., Wang, Y., Wang, W., Zhang, H., Zhang, Y.C., and Mu, L., 2010. High-resolution Lopingian (Late Permian) timescale of South China. Geological Journal, 45(2–3): 122–134.
Song, H.J., Wignall, P.B., Tong, J.N., Song, H.Y., Chen, J., Chu, D.L., Tian, L., Luo, M., Zong, K.Q., Chen, Y.L., Lai, X.L., Zhang, K.X., and Wang, H.M., 2015. Integrated Sr isotope variations and global environmental changes through the Late Permian to early Triassic. Earth and Planetary Science Letters, 424: 140–147.
Sun, Y.D., Lai, X.L., Wignall, P.B., Widdowson, M., Ali, J.R., Jiang, H.S., Wang, W., Yan, C.B., Bond, D.P.G., and Védrine, S., 2010. Dating the onset and nature of the Middle Permian Emeishan large igneous province eruptions in SW China using conodont biostratigraphy and its bearing on mantle plume uplift models. Lithos, 119(1–2): 20–33.
Tian, J.C., and Zheng. Y.F., 1995. The revolution of the isotopic composition of strontium in the Permian Paleo-oeean in South China. Acta sedimentologica Sinica, 13(4): 125–130 (in Chinese with English abstract).
Van der Meer, D.G., Van den Berg van Saparoea, A.P.H., Van Hinsbergen, D.J.J., Van de Weg, R.M.B., Goddéris, Y., Le Hir, G., and Donnadieu, Y., 2017. Reconstructing first-order changes in sea level during the Phanerozoic and Neoproterozoic using strontium isotopes. Gondwana Research, 44: 22–34.
Veevers, J.J., and Powell, C.M., 1987. Late Paleozoic glacial episodes in Gondwana land reflected in transgressive-regressive depositional sequences in Euramerica. Geological Society America Bulletin, 98(4): 475–487.
Veizer, J., 1983. Trace elements and isotopes in sedimentary carbonates. Reviews in Mineralogy and Geochemistry, 11(1): 265–299.
Veizer, J., Ala, D., Azmy, K., Bruckschen, P., Buhl, D., Bruhn, F., Carden, G.A.F., Diener, A., Ebneth, S., Goddéris, Y., Jasper, T., Korte, C., Pawellek, F., Podlaha, O.G., and Strauss, H., 1999. $^{87}Sr/^{86}Sr$, $\delta^{13}C$ and $\delta^{18}O$ evolution of Phanerozoic seawater. Chemical Geology, 161(1): 59–88.
Veizer, J., Buhl, D., Diener, A., Ebneth, S., Podlaha, O.G., Bruckschen, P., Jasper, T., Korte, C., Schaaf, M., Ala, D., and

Azmy, K., 1997. Strontium isotope stratigraphy: potential resolution and event correlation. Palaeogeography Palaeoclimatology Palaeoecology, 132(1–4): 65–77.
Vérard, C., Hochard, C., Baumgartner, P.O., Stampfli, G.M., and Liu, M., 2015. 3D palaeogeographic reconstructions of the Phanerozoic versus sea-level and Sr-ratio variations. Journal of Palaeogeography, 4(1): 64–84.
Walter, M.R., Veevers, J.J., Calver, C.R., Gorjan, P., and Hill, A.C., 2000. Dating the 840–544Ma Neoproterozoic interval by isotopes of strontium, carbon, and sulfur in seawater, and some interpretative models. Precambrian Research, 100(1–3): 371–433.
Wang, C.S., Li, X.H., Chen, H.D., and Qin, J.X., 1999. Permian Sea-level Changes and Rising-Falling Events in South China. Acta sedimentologica Sinica, 17(4): 536–541 (in Chinese with English abstract).
Wang, Q.C., and Cai, L.G., 2007. Phanerozoic tectonic evolution of South China. Acta Geologica Sinica, 81(8): 1025–1040 (in Chinese with English abstract).
Wang, W., Kano, A., Okumura, T., Ma, Y.S., Matsumoto, R., Matsuda, N., Ueno, K., Chen, X.Z., Kakuwa, Y., Gharaie, M.H.M., and Ilkhchi, M.R., 2007. Isotopic chemostratigraphy of the microbialite-bearing Permian-Triassic boundary section in the Zagros Mountains, Iran. Chemical Geology, 244(3): 708–714.
Wang, W.Q., Wang, W., Feng, X.C., Liu, X.C., Ye, F.C., Chen, Y.F., Liu, J., and Chen, X.Z., 2014. Strontium isotope stratigraphy on the division and correlation of marine sequences: An example from Lopingian marine carbonate sections. Journal of Stratigraphy, 38(4): 402–416 (in Chinese with English abstract).
Wang, X.D., and Sugiyama, T., 2000. Diversity and extinction patterns of Permian coral faunas of China. Lethaia, 33(4): 285–294.
Wickman, F.E., 1948. Isotope ratios: A clue to the age of certain marine sediments. The Journal of Geology, 56(1): 61–66.
Wierzbowski, H., Anczkiewicz, R., Pawlak, J., Rogov, M.A., and Kuznetsov, A.B., 2017. Revised Middle-Upper Jurassic strontium isotope stratigraphy. Chemical Geology, 466: 239–255.
Williamson, T., Henderson, R.A., Price, G.D., and Collerson, K.D., 2012. Strontium-isotope stratigraphy of the Lower Cretaceous of Australia. Cretaceous Research, 36: 24–36.
Xiao, J.F., Li, R.X., Wang, X.L., and Wei, J.Y., 2009. The characteristics of strontium isotopes composition about Permian—Triassic boundary in the great bank of Guizhou. Geological Review, 55(5): 647–652 (in Chinese with English abstract).
Xu, W., Xu, X.Y., Niu, Y.Z., Song, B., Chen, G.C., Shi, J.Z., Zhang, Y.X., and Li, C.H., 2019. Geochronology and petrogenesis of the Permian marine basalt in the southern Beishan region and their tectonic implications. Acta Geologica Sinica, 93(8): 1928–1953 (in Chinese with English abstract).
Xu, Y.G., Luo, Z.Y., Huang, X.L., He, B., Xiao, L., Xie, L.W., and Shi, Y.R., 2008. Zircon U-Pb and Hf isotope constraints on crustal melting associated with the Emeishan mantle plume. Geochimica et Cosmochimica Acta, 72(13): 3084–3104.
Yan, S.T., Qin, M., Duan, Y.H., and Wen, L., 2019. Identification of the Permian ocean island rock association from the Litang Area in Sichuan Province and its tectonic significance: Evidence from petrology, geochemistry and geochronology. Acta Geologica Sinica, 93(2): 381–393 (in Chinese with English abstract).
Yang, Y.Q., and Feng, Z.Z., 2000. Permian depositional systems in south China. Journal of Palaeogeography (Chinese Edition), 2(1): 1–11 (in Chinese with English abstract).
Ye, F.C., Liu, X.C., Wang, W., Chen, X.Z., Liu, J., Shen, S.Z., Wang, W.Q., Wang, X.D., Wang, Y., Cao, C.Q., Zheng, Q.F., Zhang, H., and Zhang, Y.C., 2015. Biostratigraphy constraining strontium isotopic stratigraphy and its application on the Lopingian (Late Permian). Science China: Earth Sciences, 58(11): 1951–1959.
Zhang, H., Cao, C.Q., Liu, X.L., Mu, L., Zheng, Q.F., Liu, F., Xiang, L., Liu, L.J., and Shen, S.Z., 2015. The terrestrial end-Permian mass extinction in South China. Palaeogeography Palaeoclimatology Palaeoecology, 448: 108–124.
Zhang, L.Q., 2013. Palaeoenvironmental change across the Guadalupian–Wuchiapingian boundary in Sichuan, South China. Acta Geologica Sinica (English Edition), 87(z1): 880–882.
Zhang, Y.L, Jia, X.T., and Wang, Z.Q., 2019. Provenance of the Late Permian Xuanwei Formation in the Upper Yangtze Block: Constraints from the Sedimentary Record and Tectonic Implications. Acta Geologica Sinica (English Edition), 93(6): 1673–1686.
Zhang, Z.C., Mahoney, J.J., Mao, J.W., and Wang, F.S., 2006. Geochemistry of picritic and associated basalt flows of the western Emeishan flood basalt province, China. Journal of Petrology, 47(10): 1997–2019.
Zheng, L.D., Yang, Z.Y., and Tong, Y.B., 2010. Magnetostratigraphic constraints on two-stage eruptions of the Emeishan continental flood basalts. Geochemistry Geophysics Geosystems, 11(12): 1–70.
Zhong, Y.T., He, B., Mundil, R., Xu, Y.G., 2014. CA-TIMS zircon U-Pb dating of felsic ignimbrite from the Binchuan section: Implications for the termination age of Emeishan large igneous province. Lithos, 204(3): 14–19.
Zhou, M.F., Malpas, J., Song, X.Y., Robinson, P.T., Sun, M., Kennedy, A.K., Lesher, C.M., and Keays, R.R., 2002. A temporal link between the Emeishan large igneous province (SW China) and the end-Guadalupian mass extinction. Earth and Planetary Science Letters, 196(3–4): 113–122.
Zhu, X.M., Yang, J.S., and Zhang, X.L., 2004. Application of lithofacies palaeogeography in petroleum exploration. Journal of Palaeogeography, 6(1): 101–109 (in Chinese with English abstract).

About the first author

QU Hongjun, male, born in 1967 in Baoji City, Shaanxi Province; Ph.D.; graduated from Northwest University; professor of Department of Geology, Northwest University, China. He is mainly engaged in the research of sedimentology. Email: hongjun@nwu.edu.cn; phone: 13772500178.

About the corresponding author

CHEN Shuo, male, born in 1994 in Xi'an City, Shaanxi Province; Master's Degree; Ph.D student of Department of Geology, Northwest University, China. He is mainly engaged in the research of sedimentology. Email: nwu_chenshuo@163.com; phone: 18729064974.